View metadata, citation and similar papers at core.ac.uk
brought to you by CORE
provided by PolyU Institutional Repository

Orientation relationships between TiB (B27), B2, and Ti_3Al phases

C.L. Chen
Shenyang National Laboratory for Materials Science, Institute of Metal Research, Chinese Academy of Sciences, Shenyang 110016, People's Republic of China; and Research Center for Ultra-High Voltage Electron Microscopy, Osaka University, Osaka, Japan

W. Lu
Shenyang National Laboratory for Materials Science, Institute of Metal Research, Chinese Academy of Sciences, Shenyang 110016, People's Republic of China; and Department of Applied Physics, The Hong Kong Polytechnic University, Hung Hom, Kowloon, Hong Kong, People's Republic of China

L.L. He[a] and H.Q. Ye
Shenyang National Laboratory for Materials Science, Institute of Metal Research, Chinese Academy of Sciences, Shenyang 110016, People's Republic of China

(Received 27 August 2008; accepted 17 November 2008)

The orientation relationships among TiB (B27), B2, and Ti_3Al phases have been investigated by transmission electron microscopy. By using the composite selected-area electron diffraction technique, the orientation relationship between TiB (B27) and B2 was determined to be $[100]_{TiB}||[001]_{B2}$, $(001)_{TiB}||(010)_{B2}$; and that between TiB (B27) and Ti_3Al was $[010]_{TiB}||[1120]_{Ti_3Al}$, $(001)_{TiB}||(0001)_{Ti_3Al}$. These orientation relationships have been predicted precisely by the method of coincidence of reciprocal lattice points.

I. INTRODUCTION

TiAl alloys are promising materials for application in aerospace and automotive engine components due to their low-density and good high-temperature properties.[1–3] Extensive efforts have been devoted to studying their possible technological applications in past decades.[4–6] It is suggested that the addition of boron in TiAl has two effects that can significantly improve the mechanical properties of TiAl alloys[7,8]: one is grain refinement, and the other is dispersion strengthening by borides. The effect of grain refinement of boron in TiAl alloys can be summarized as follows[9]: on one hand, there is a minimum boron level required for grain refinement, and it is alloy composition-dependent. If the boron concentration is below this critical level, no grain refinement can be achieved: on the other hand, as soon as the alloys are fully grain refined, any excess boron concentration does not contribute to a further reduction in grain size. Because the morphologies and structures of borides have a significant impact on the properties of TiAl alloys with boron addition, much effort has been devoted to investigating the morphologies and structures of borides in TiAl alloys. The morphologies ranging from needle through flake to block particles have been reported in different alloy systems.[10–12] For the categories of borides, both monoborides and diborides have been found in TiAl alloys with the addition of boron. It has been proposed that the strong boride formers, such as W, Ta, and Nb, change the prevalent titanium boride form from TiB_2 to TiB.[13]

In the past, the orientation relationships of borides with α, β, and γ phases have been widely investigated.[11,14] However, although it is also of significant importance, the orientation relationship between TiB and α_2-Ti3Al is still unknown. On the other hand, although B.J. Inkson et al.[15] revealed the orientation relationship between TiB_2 and B2, and U. Kitkamthorn et al.[16,17] examined the orientation relationship between TiB (B_f) and B2, the orientation relationship between TiB (B27) and B2 has not been reported. (TiB phase has two kinds of structures, Bf and B27.[15]) Therefore, in the present study, the orientation relationships between TiB (B27), B2, and Ti_3Al phases have been investigated using transmission electron microscopy (TEM). These orientation relationships have been predicted precisely by the method of coincidence of reciprocal lattice points (CRLP).

II. EXPERIMENTAL

The alloy with nominal composition of Ti–45Al–8Nb–0.2W–0.2B–0.02Y (at.%) was prepared using the consumable electrode arc-melting technique under argon protection, and it was remelted in a vacuum skull melting furnace to reduce composition heterogeneity. An ingot with a diameter of 120 mm and a height of 420 mm was cast, and then hot isostatic was pressed to eliminate casting porosity. Chemical analyses indicated that

[a]Address all correspondence to this author.
e-mail: llhe@imr.ac.cn
DOI: 10.1557/JMR.2009.0220

 © 2009 Materials Research Society
http://journals.cambridge.org Downloaded: 22 Oct 2013 IP address: 158.132.161.52

the composition of the ingot matched the nominal composition within the experimental error. The forging billet was machined from the ingot, canned, and forged at the ($\alpha + \gamma$) phase region to a height reduction of more than 75%. For the TEM observation, slices of approximately 0.4-mm thickness were cut from the as-forged alloys. The slices were mechanically ground from both sides to approximately 30 μm and then thinned by standard twin-jet polishing or ion milling. The thin foils were examined in a JEOL-2010 high-resolution transmission electron microscope (Tokyo, Japan).

III. RESULTS AND DISCUSSION

Although TiB phase has two kinds of structures, namely Bf and B27, the TiB precipitate in the present study has the B27 structure. Figure 1 shows an example of a B2 particle ($Ti_{51}Al_{33}Nb_{16}$ at.%) precipitating from TiB (B27) phase (a) and the corresponding composite selected-area electron diffraction pattern (b), from which their orientation relationship can directly be written as:

$$[100]_{TiB}||[001]_{B2}, (001)_{TiB}||(010)_{B2} \quad . \qquad (1)$$

One can note that there are lots of stacking faults in the TiB (B27) particle that cause the elongation of its diffraction patterns along $(001)_{TiB}$ direction. Likewise, Fig. 2 shows a TiB (B27) plate precipitating from α_2-Ti_3Al phase (a) and the corresponding composite selected-area electron diffraction pattern (b), from which their orientation relationship can directly be written as:

$$[010]_{TiB}||[1120]_{Ti_3Al}, (001)_{TiB}||(0001)_{Ti_3Al} \quad . \qquad (2)$$

In the following, we shall show that these orientation relationships can be predicted by CRLP, which has been proved to be powerful and accurate in analyzing orientation relationships between two adjoining crystals.[18–21] The CRLP method was first proposed by Ikuhara and Pirouz,[18] in which the overlap of reciprocal lattice points (RLP) of two adjoining crystals is used to obtain a geometrically optimum orientation relationship between the two crystals. Each RLP, corresponding to the reciprocal lattice vector **g**, is represented by a sphere of radius r* around the reciprocal lattice point. It is then hypothesized that the orientation relationship favored between two adjoining crystals is the one in which the sum of the overlapping volumes is maximized. Given the primitive unit cell parameters of the two adjoining lattices and the radius r*, the sum of all overlapping volumes V(θ, ψ) is calculated as a function of rotations θ and ψ about the orthogonal axes of one of the lattices. Assuming that the origins of the reciprocal lattices of the two crystals are coincident in the three-dimensional (3-D) reciprocal space, one of the crystals is rotated. The summation in V(θ, ψ) is carried out over all RLPs up to a maximum distance R* in the composite reciprocal lattice. Then, V(θ, ψ) is plotted against (θ, ψ). In all of the cases that have been calculated, the main peaks in the plots represent the preferential orientation relationships. In the two variances r* and R*, the maximum distance R* has little influence on the calculation results if its value is large enough; however, a smaller radius r* will improve the distinguishability of the plots.

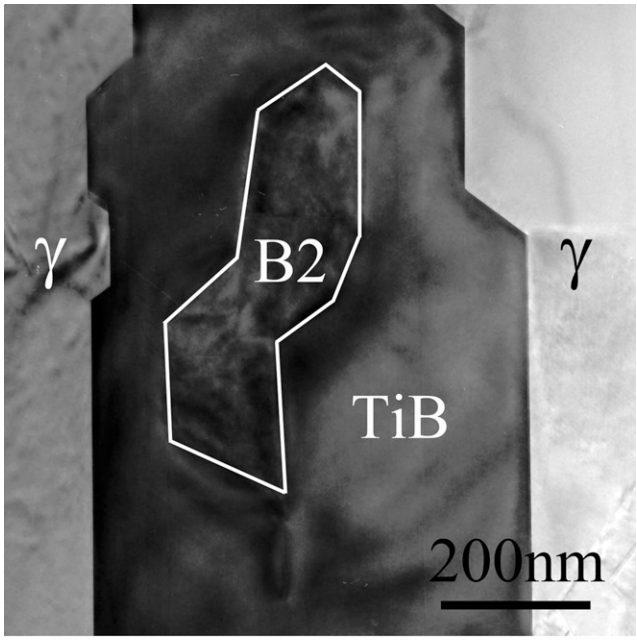

(a)

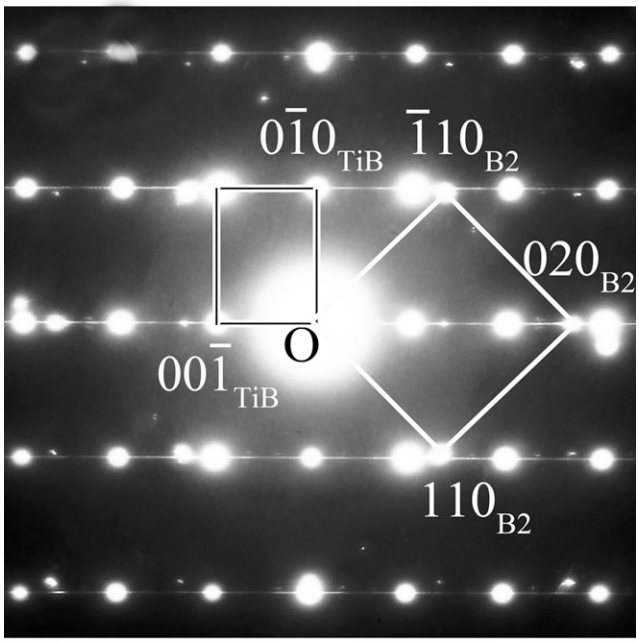

(b)

FIG. 1. Bright-field image showing (a) the precipitating of B2 from TiB (B27) phase, and (b) the corresponding composite selected-area electron diffraction pattern. The contours of B2 are underlined. The orientation relationship can be described as $[100]_{TiB}||[001]_{B2}$, $(001)_{TiB}||(010)_{B2}$.

CAMBRIDGE JOURNALS
http://journals.cambridge.org Downloaded: 22 Oct 2013 IP address: 158.132.161.52

We have computed and plotted V (θ, ψ) versus (θ, ψ) for the TiB (B27)/B2 and TiB (B27)/Ti_3Al systems, respectively. To simplify the calculation and the plots, it is useful to consider the symmetry of the reciprocal lattices. For TiB (B27) with space group Pnma, the reciprocal lattice has a point group of mmm, which means that the V (θ, ψ)-(θ, ψ)ℊ plot should have a minimum repetitive unit in the range of θ ℊ = 0–90° and ψ = 0–90°, the residual parts of plot can be obtained by its symmetry operations. Therefore, only the part of 3Dℊ plot corresponding to θ = 0–90° and ψ = 0–90° is shown in the present article.

The calculation of TiB (B27)/B2 system started from the orientation as shown in Fig. 3(a). The low-index directions of the two crystals are set to be parallel, i.e., $[100]_{TiB}||[001]_{B2}$ and $[001]_{TiB}||[010]_{B2}$. In fact, the initial orientation can be random. As shown in Fig. 3(b), the calculated 3Dℊ plot of TiB (B27)/B2 system has five predominant peaks (No. 1 ∼ No. 5), which appear at

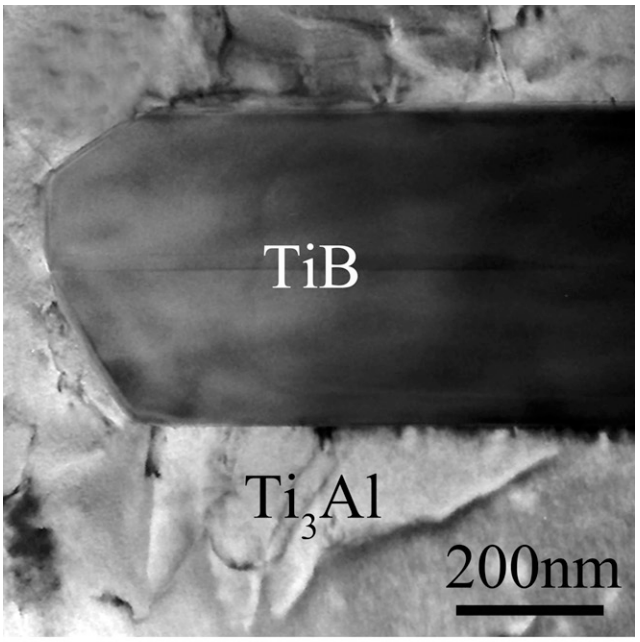

(a)

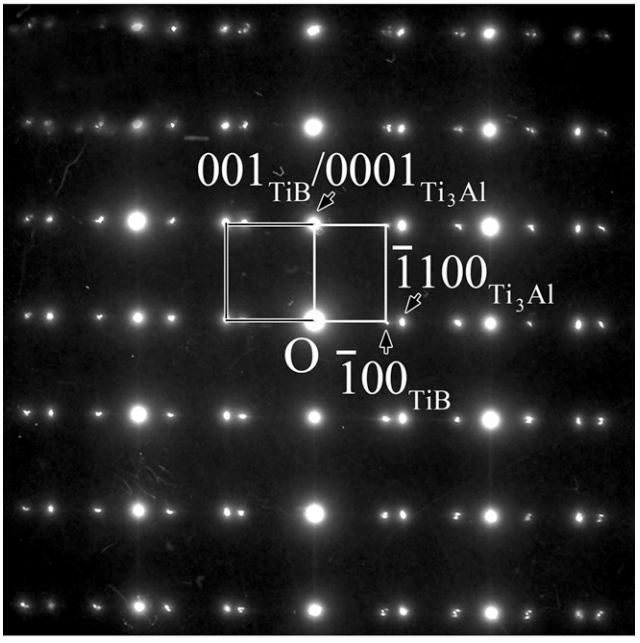

(b)

FIG. 2. Bright-field image showing (a) the precipitating of TiB (B27) from Ti_3Al phase, and (b) the corresponding composite selected-area electron diffraction pattern. The orientation relationship can be described as $[010]_{TiB}||[11\bar{2}0]_{Ti_3Al}$, $(001)_{TiB}||(0001)_{Ti_3Al}$.

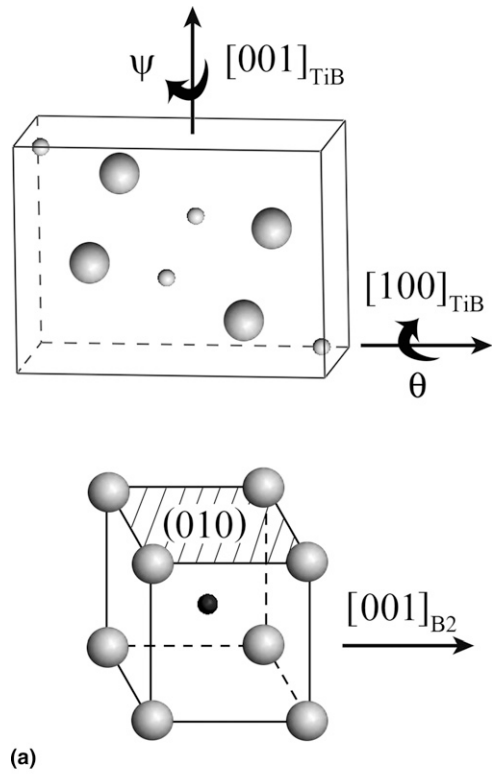

(a)

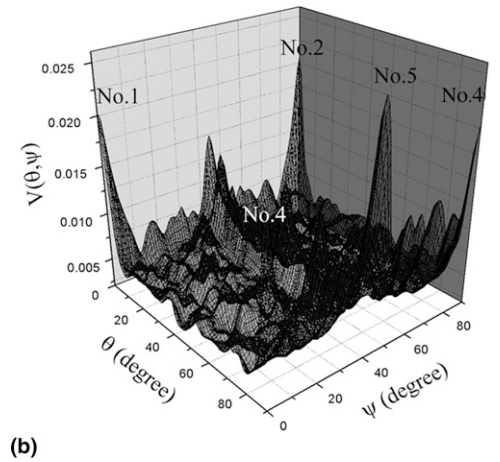

(b)

FIG. 3. (a) Assumed orientation relationship from which the calculation of TiB (B27)/B2 system started, (b) 3-D plot of V(θ, ψ) for rotations of θ and ψ (r* = 0.1a*, R* = 3a*). Note that the five main peaks (No. 1 ∼ No. 5) correspond to the preferential orientation relationships.

http://journals.cambridge.org Downloaded: 22 Oct 2013 IP address: 158.132.161.52

$\theta_1 = 0°$, $\psi_1 = 0°$; $\theta_2 = 0°$, $\psi_2 = 90°$; $\theta_3 = 90°$, $\psi_3 = 90°$; $\theta_4 = 90°$, $\psi_4 = 0°$; and $\theta_5 = 90°$, $\psi_5 = 45°$, respectively. Because B2 structure has a tetrad axis along <001> directions, the main peaks from No. 1 to No. 4 are equivalent, which correspond to the orientation relationship of Eq. (1). The other strong peak (No. 5, $\theta_5 = 90°$, $\psi_5 = 45°$) represents the orientation relationship of $[304]_{TiB}||[001]_{B2}$, $(010)_{TiB}||(010)_{B2}$ that may also exist, although it has not been observed in the present study. Likewise, the calculation of TiB (B27)/Ti_3Al system started from the orientation as shown in Fig. 4(a). The

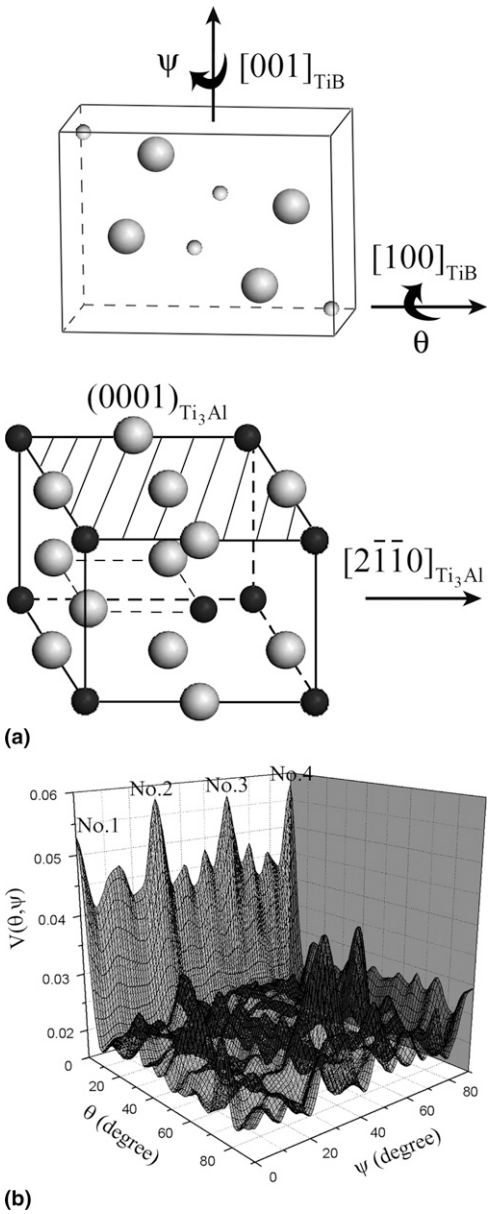

FIG. 4. (a) Assumed orientation relationship from which the calculation of TiB (B27)/Ti_3Al system started, (b) 3-D plot of V(θ, ψ) for rotations of θ and ψ (r* = 0.15a*, R* = 3a*). Note that the four main peaks (No. 1 ~ No. 4) correspond to the preferential orientation relationships.

low-index directions of the two crystals are set to be parallel, i.e., $[001]_{TiB}||[0001]_{Ti_3Al}$ and $[100]_{TiB}||[2\bar{1}\bar{1}0]_{Ti_3Al}$ As shown in Fig. 4(b), the calculated 3D plot of TiB (B27)/Ti_3Al system has four predominant peaks (No. 1 ~ No. 4), which appear at $\theta_1 = 0°$, $\psi_1 = 0°$; $\theta_2 = 0°$, $\psi_2 = 30°$; $\theta_3 = 0°$, $\psi_3 = 60°$; and $\theta_4 = 0°$, $\psi_4 = 90°$, respectively. Because α_2-Ti_3Al structure has a hexad axis along [0001] direction, the peaks No. 1 and No. 3 and No. 2 and No. 4 are equivalent, respectively. The peaks No. 2 and No. 4 correspond to the orientation relationship of Eq. (2). The other two strong peaks (No. 1 and No. 3) correspond to the orientation relationship of $[010]_{TiB}||<01\bar{1}0>_{Ti_3Al}$, $(001)_{TiB}||(0001)_{Ti_3Al}$ that may also exist, although it has not been observed in the present study.

The edge-to-edge matching model developed by Zhang and Kelly[22–24] also has the ability to predict the orientation relationships for a given system based on the crystal structures. It is interesting to compare the results predicted by CRLP and those by the edge-to-edge matching model. According to the edge-to-edge matching model, the interatomic spacing misfit (%) along matching directions should be less than a critical value 10%, and the d-value mismatch (%) between possible matching planes should be less than 6%. Applying to the systems in this article, the interatomic spacing misfit (%) along matching directions $[100]_{TiB}||[001]_{B2}$ and $[010]_{TiB}||[11\bar{2}0]_{Ti_3Al}$ are −3.3 and 6.5%, respectively. They fit the critical value of the edge-to-edge matching model (<10%). The d-value mismatch (%) between possible matching planes $(003)_{TiB}||(020)_{B2}$ and $(001)_{TiB}||(0001)_{Ti_3Al}$ are −3.9 and −1.8%, respectively. They also fit the critical value of the edge-to-edge matching model (<6%). Therefore, the edge-to-edge matching model will give a similar orientation relationships as those by CRLP.

IV. CONCLUSIONS

In the present study, the orientation relationships among TiB (B27), B2, and Ti_3Al phases have been investigated by transmission electron microscopy. Through the analyses of composite selected-area electron-diffraction patterns, the orientation relationship between TiB (B27) and B2 was determined to be $[100]_{TiB}||[001]_{B2}$, $(001)_{TiB}||(010)_{B2}$; and that between TiB (B27) and Ti_3Al was $[010]_{TiB}||[11\bar{2}0]_{Ti_3Al}$, $(001)_{TiB}||(0001)_{Ti_3Al}$. According to the calculations by CRLP, these orientation relationships were attributed to the largest overlap of their reciprocal lattices.

ACKNOWLEDGMENTS

This research was supported by the National Natural Science Foundation of China (Grant No. 50271073) and the Major State Basic Research Projections of China (Grant No. 2006CB600905). We gratefully acknowledge this support.

CAMBRIDGE JOURNALS
http://journals.cambridge.org Downloaded: 22 Oct 2013 IP address: 158.132.161.52

REFERENCES

1. Y.W. Kim: Ordered intermetallic alloys. Part III: Gamma titanium aluminides. *JOM* **96,** 30 (1994).
2. F. Appel, U. Sparka, and R. Wagner: Work hardening and recovery of gamma base titanium aluminides. *Intermetallics* **7,** 325 (1999).
3. K. Maruyama, M. Yamaguchi, G. Suzuki, H.L. Zhu, H.Y. Kim, and M.H. Yoo: Effects of lamellar boundary structural change on lamellar size hardening in TiAl alloy. *Acta Mater.* **52,** 5185 (2004).
4. F. Appel and R. Wagner: Microstructure and deformation of two-phase γ-titanium aluminides. *Mater. Sci. Eng., R* **22,** 187 (1998).
5. M. Yamaguchi, H. Inui, and K. Ito: High-temperature structural intermetallics. *Acta Mater.* **48,** 307 (2000).
6. H.A. Calderon, V. Garibay-Febles, M. Umemoto, and M. Yamaguchi: Mechanical properties of nanocrystalline Ti–Al–X alloys. *Mater. Sci. Eng., A* **329–331,** 196 (2002).
7. D. Hu: Effect of boron addition on tensile ductility in lamellar TiAl alloys. *Intermetallics* **10,** 851 (2002).
8. U. Hecht, V. Witusiewicz, A. Drevermann, and J. Zollinger: Grain refinement by low boron additions in niobium-rich TiAl-based alloys. *Intermetallics* **16,** 969 (2008).
9. T.T. Cheng: The mechanism of grain refinement in TiAl alloys by boron addition-an alternative hypothesis. *Intermetallics* **8,** 29 (2000).
10. M.E. Hyman, C. McCullough, J.J. Valencia, C.G. Levi, and R. Mehrabian: Microstructure evolution in TiAl alloys with B additions. Conventional solidification. *Metall. Trans. A* **20,** 1847 (1989).
11. M.E. Hyman, C. McCullough, C.G. Levi, and R. Mehrabian: Evolution of boride morphologies in TiAl-B alloys. *Metall. Trans. A* **22,** 1647 (1991).
12. M. De Graef, J.P.A. Lofvander, and C.G. Levi: The structure of complex monoborides in γ-TiAl alloys with Ta and B additions. *Acta Metall. Mater.* **39,** 2381 (1991).
13. D. Hu: Effect of composition on grain refinement in TiAl-based alloys. *Intermetallics* **9,** 1037 (2001).
14. C.L. Chen, W. Lu, J.P. Lin, L.L. He, G.L. Chen, and H.Q. Ye: Orientation relationship between TiB precipitate and γ-TiAl phase. *Scr. Mater.* **56,** 441 (2007).
15. B.J. Inkson, C.B. Boothroyd, and C.J. Humphreys: Boride morphology in a (Fe, V, B) Ti-alloy containing B2-phase. *Acta Metall. Mater.* **43,** 1429 (1995).
16. U. Kitkamthorn, L.C. Zhang, T.T. Aindow, and M. Aindow: The structure of ribbon borides in a Ti-44Al-4Nb-4Zr-1B alloy. *Microsc. Microanal.* **11**(Suppl 2), 1702 (2005).
17. U. Kitkamthorn, L.C. Zhang, and M. Aindow: The structure of ribbon borides in a Ti-44Al-4Nb-4Zr-1B alloy. *Intermetallics* **14,** 759 (2006).
18. Y. Ikuhara and P. Pirouz: Orientation relationship in large mismatched bicrystals and coincidence of reciprocal lattice points (CRLP). *Mater. Sci. Forum* **207–209,** 121 (1996).
19. P. Pirouz, F. Ernst, and Y. Ikuhara: On epitaxy and orientation relationships in bicrystals. *Diffus. Defect Data B Solid State Phenom.* **59–60,** 51 (1998).
20. S. Stemmer, P. Pirouz, I. Ikuhara, and R.F. Davis: Film/substrate orientation relationship in the AIN/6H-SiC epitaxial system. *Phys. Rev. Lett.* **77,** 1797 (1996).
21. R. Yu, L.L. He, J.T. Guo, H.Q. Ye, and V. Lupinc: Orientation relationship and interfacial structure between ζ-Ti_5Si_3 precipitates and γ-TiAl intermetallics. *Acta Mater.* **48,** 3701 (2000).
22. M-X. Zhang and P.M. Kelly: Edge-to-edge matching model for predicting orientation relationships and habit planes—The improvements. *Scr. Mater.* **52,** 963 (2005).
23. M-X. Zhang and P.M. Kelly: Edge-to-edge matching and its applications. Part I. Application to the simple HCP/BCC system. *Acta Mater.* **53,** 1073 (2005).
24. M-X. Zhang and P.M. Kelly: Edge-to-edge matching and its applications. Part II. Application to Mg–Al, Mg–Y and Mg–Mn alloys. *Acta Mater.* **53,** 1085 (2005).

http://journals.cambridge.org Downloaded: 22 Oct 2013 IP address: 158.132.161.52